Molecular Pharmacology Fast Forward. Published on May 26, 2015 as DOI: 10.1124/mol.115.098541
This article has not been copyedited and formatted. The final version may differ from this version.

Structural Basis of Species-dependent Differential Affinity of 6-Alkoxy-5-aryl-3-pyridinecarboxamide Cannabinoid Receptor 1 Antagonists

Malliga R. Iyer, Resat Cinar, Jie Liu, Grzegorz Godlewski, Gergő Szanda, Henry Puhl, Stephen R. Ikeda, Jeffrey Deschamps, Yong-Sok Lee, Peter J. Steinbach, and George Kunos

Laboratory of Physiologic Studies (M.R.I., R.C., J.L., G.G., G.S., G.K.) and Laboratory of Molecular Physiology (H.P., S.R.I.), National Institute on Alcohol Abuse and Alcoholism, National Institutes of Health, Bethesda, MD 20892; Naval Research Laboratory, Washington, DC 20375 (J.D.); and Center for Molecular Modeling, Center for Information Technology, National Institutes of Health, Bethesda, MD 20892 (Y.S.L., P.J.S.)

Molecular Pharmacology Fast Forward. Published on May 26, 2015 as DOI: 10.1124/mol.115.098541
This article has not been copyedited and formatted. The final version may differ from this version.

Running Title: Species-specific affinity of CB1 receptor antagonists.

Correspondence: George Kunos, Laboratory of Physiologic Studies, National Institute on Alcohol Abuse and Alcoholism, Bethesda, MD 20892-9413. E-mail: george.kunos@nih.gov

Number of text pages: 21 (including figure legends)

Tables: 0

Figures: 5

References: 36

Number of words in abstract: 125

Introduction: 565

Results and Discussion: 1678

ABBREVIATIONS: **14g**, 5-(4-chlorophenyl)-6-(cyclopropylmethoxy)-N-[(1*R*,2*R*)-2-hydroxy-cyclohexyl]-3-pyridinecarboxamide; **14h**, 5-(4-chlorophenyl)-N-[(1*R*,2*R*)-2-hydroxycyclohexyl]-6-(2-methoxyethoxy)-3-pyridinecarboxamide; CB_1R, cannabinoid receptor 1; DIO, diet-induced obesity;

Molecular Pharmacology Fast Forward. Published on May 26, 2015 as DOI: 10.1124/mol.115.098541
This article has not been copyedited and formatted. The final version may differ from this version.

Abstract

6-Alkoxy-5-aryl-3-pyridincarboxamides, including the brain penetrant compound **14g** and its peripherally restricted analog **14h**, have been recently introduced as selective, high affinity antagonists of the human cannabinoid receptor-1 (hCB_1R, J. Med. Chem. 56, 9874-96, 2013). Binding analyses revealed two orders of magnitude lower affinity of these compounds for mouse and rat versus human CB_1R, whereas the affinity of rimonabant is comparable for all three CB_1Rs. Modeling of ligand binding to CB_1R and binding assays with native and mutant (Ile105Met) hCB_1Rs indicate that the Ile105 to Met mutation in rodent CB_1Rs accounts for the species-dependent affinity of **14g** and **14h**. Our work identifies Ile105 as a new pharmacophore component for developing better hCB_1R antagonists and invalidates rodent models for assessing the antiobesity efficacy of **14g** and **14h**.

Molecular Pharmacology Fast Forward. Published on May 26, 2015 as DOI: 10.1124/mol.115.098541
This article has not been copyedited and formatted. The final version may differ from this version.

Introduction

An overactive endocannabinoid/CB_1R system has been implicated in obesity and its metabolic complications (Bluher et al., 2006; Pacher et al., 2006). Globally acting CB_1R antagonists reduce body weight and hepatic fat accumulation and improve insulin sensitivity and dyslipidemia in overweight people with the metabolic syndrome (Despres et al., 2005; Pi-Sunyer et al., 2006), but their therapeutic development was halted due to neuropsychiatric side effects (Le Foll et al., 2009). However, CB_1R in peripheral tissues, including adipose tissue, liver, skeletal muscle, pancreatic β-cells and tissue macrophages contribute to the metabolic effects of endocannabinoids (Cota et al., 2003; Jourdan et al., 2013; Kim et al., 2011; Liu et al., 2005; Osei-Hyiaman et al., 2005), suggesting that selective blockade of peripheral CB_1R may provide a therapeutic alternative by avoiding side effects linked to blockade of CB_1R in the CNS. Indeed, several recent studies documented that when tested in rodent models of obesity/metabolic syndrome and type-2 diabetes, novel CB_1R antagonists with very low brain penetrance are devoid of behavioral effects predictive of neuropsychiatric side effects in humans, yet have retained most if not all the metabolic efficacy of globally acting CB_1R antagonists (Jourdan et al., 2013; Tam et al., 2012; Tam et al., 2010).

In a recent study, 6-alkoxy-5-aryl-3-pyridinecarboxamides have been introduced as a new series of orally bioavailable CB_1R antagonists with low nanomolar affinity for the human CB_1R (Röver et al., 2013). Two analogs were tested in that study, one with high and one with low brain penetrance (brain:plasma ratios of 1.3 versus 0.13, respectively) in a rat model of high-fat diet-induced obesity (DIO) and found that the analog with high brain penetrance (5-(4-chlorophenyl)-6-(cyclopropylmethoxy)-N-[(1*R*,2*R*)-2-hydroxycyclohexyl]-3-pyridinecarbox-amide, designated as **14g,** see Fig. 1) caused significant delays in weight gain and adiposity, but the analog with low brain penetrance (5-(4-chlorophenyl)-N-[(1*R*,2*R*)-2-hydroxycyclohexyl]-6-(2-methoxyethoxy)-3-pyridinecarboxamide, designated as **14h,** see Fig.

Molecular Pharmacology Fast Forward. Published on May 26, 2015 as DOI: 10.1124/mol.115.098541
This article has not been copyedited and formatted. The final version may differ from this version.

1) did not. This had led the authors to the conclusion that the antiobesity efficacy of CB_1R blockade is primarily centrally mediated (Röver et al., 2013).

The high-fat fed rats used in the above study represent a weak model of the metabolic syndrome as only a subset of the animals develops modest weight gain beyond the normal growth of the animals, and they do not display an increase in the accumulation of ectopic fat in the liver or changes in plasma leptin and insulin concentrations, which would indicate insulin or leptin resistance (Flamment et al., 2009; Röver et al., 2013). We wanted to test the effects of the above two compounds in DIO mice, a more robust model of the metabolic syndrome (Collins et al., 2004), for which we needed to establish their affinities for the mouse CB_1R. Unexpectedly, we found that the binding affinity (K_i) of both compounds was one to two orders of magnitude lower for both the mouse and rat CB_1R relative to their affinities for the human CB_1R, and accordingly failed to elicit CB_1R blockade in functional assays *in vivo*. This prompted us to analyze these ligands along with the reference compound rimonabant, which has equal high CB_1R binding affinity in the 3 species (Govaerts et al., 2004), for their interaction with mouse, rat and human CB_1R, using molecular modeling. The resulting binding model, strongly supported by site-directed mutagenesis of a key residue in human vs mouse CB_1R, provides the likely structural basis of these striking species-dependent differences, unprecedented among other CB_1R ligands introduced to date (Govaerts et al., 2004; Thomas et al., 2005).

Molecular Pharmacology Fast Forward. Published on May 26, 2015 as DOI: 10.1124/mol.115.098541
This article has not been copyedited and formatted. The final version may differ from this version.

Materials and Methods

CB_1R Antagonists. Compounds **14g** and **14h** were synthesized as described (Röver et al., 2013). The correct structure was verified by NMR spectroscopy and, for compound **14h**, by X-ray crystallography (Supplemental Figure 1). Rimonabant (SR141716) was provided by the NIDA Drug Supply Program.

X-ray Diffraction. Details provided in supplemental materials.

CB_1R Binding Assays. The binding affinity of different antagonists/inverse agonists was determined in radioligand displacement assays using 1nM of [^{3}H]CP55940 as the agonist radioligand and plasma membrane preparations from mouse or rat brain or from Chinese hamster ovary (CHO) cells transfected with the cDNA encoding the human CB_1R. K_i values were derived by computerized curve fitting and using the Cheng-Prusoff equation to account for the affinity of the radioligand by using the GraphPad Prism 6 program (GraphPad Prism Software In., San Diego, CA). Non-specific binding was determined in the presence of 1 μM rimonabant and accounted for <20% of total binding. Plasma membranes were prepared as described from mouse and rat brain (Compton et al., 1993) and from cultured CHO-K1 cells (Perkin Elmer, MA).

CB_1R Functional Antagonism. The inhibitory potency of antagonists/inverse agonists was determined by the concentration-dependent inhibition of 1 μM CP55940-stimulated [^{35}S]GTPγS binding, assayed as described earlier (Griffin et al., 1998). In some assays, full agonist dose-response curves were generated in the absence or presence of increasing concentrations of antagonists to generate Schild-plots for testing the competitive nature of the antagonism (Sim-Selley et al., 2001). Concentration-response relations were analyzed by sigmoidal curve fitting using the GraphPad Prism 6 program. Mouse brain crude membrane fractions (10 μg) were incubated with 0.05 nM [^{35}S]GTPγS and the indicated concentrations of ligands in TEM buffer (50 mM Tris–HCl, 0.2 mM EGTA and 9 mM $MgCl_2$, pH 7.4) containing 100 μM GDP, 150 mM NaCl and 0.1% (w/v) BSA in a total volume of 1 mL for 60 min at 30°C. Nonspecific binding was determined in the presence of 10 μM GTPγS, and at baseline it represented <10% of total binding. Agonist-stimulated GTPγS binding was expressed as % increase over baseline. Bound and free [^{35}S]GTPγS were separated by vacuum filtration through Whatman GF/B filters using a Brandel M24 Cell Harvester (Gaithersburg, MD, USA). Filters were washed with 3 X 5 mL of ice-cold buffer, and radioactivity was detected by scintillation spectrometry (LS6500; Beckman Coulter).

Molecular Pharmacology Fast Forward. Published on May 26, 2015 as DOI: 10.1124/mol.115.098541
This article has not been copyedited and formatted. The final version may differ from this version.

Ligand Modeling. The X-ray structure of **14h** (Supplemental Figure 1) was used as a template to build **14g**. The compound **32a** was built based on the structure shown in (Röver et al., 2013). The conformers of these ligands were obtained by varying the dihedral angle φ as defined in Fig. 3A while relaxing the rest of the structure at the level of B3LYP/6-31G* as implemented in the Gaussian 09 software (Frisch et al., 2009). The X-ray structure of rimonabant was retrieved from the Cambridge Crystallographic Data Centre as CCDC 924604 (Perrin et al., 2013). Its 2,4-dichlorophenyl ring was then rotated with respect to the C1-N1 bond axis, and a more stable conformer was used for a docking study. Each of the conformers in the study was fully geometry optimized without any constraint. The calculated Gibbs free energy of each conformer includes the electronic energy as well as the thermal and entropy contribution at 298.15K.

CB_1R Modeling. A model of human CB_1R was built using the Prime software (Schrodinger, LLC). The crystal structure of the sphingosine 1-phosphate receptor fused to T4-lysozyme with a sphingolipid mimic bound was chosen as the template (pdb code: 3V2W) (Hanson et al., 2012). Of the 293 residues modeled in CB_1R (ranging from F89 to M411), 83 (28 %) are nearest to identical residues in the template structure (Data Supplement 1).

Human and Mouse *CNR1* Mutagenesis. The human *CNR1* (NM_007726) open reading frame was inserted into the mammalian expression vector pCI (Promega). The mouse *Cnr1* (NM_0011602586) open reading frame in pcDNA3 (Life Technologies) was kindly provided by Dr. Mary E. Abood. Mutagenesis was performed using the QuikChange site directed mutagenesis system from Agilent. The human *CNR1* was mutated at amino acid position 105 from Ile to Met using the following primer and its complement (mutated codon is indicated): *hCNR1* I105M: 5'-GAGAACTTCATGGACATGGAGTGTTTCATGGTC-3'. The mouse *Cnr1* was mutated at amino acid position 106 from Met to Ile using the following primer and its complement: mCnr1 M106I: 5'-GGAGAATTTTATGGACATAGAGTGCTTCATGATTCTG-3'. Mutations were verified by sequence analysis (Macrogen USA) and plasmids were prepared using the QIAfilter Plasmid Maxi Kit (Qiagen).

Cell Culture and Plasmid Transfection. HEK293 cells (ATCC) were maintained in EMEM with 10% FBS. Cells were transfected with different plasmids (hCB_1R-Ile105, hCB_1R-mutant met105, mCB_1R-met106, and mCB_1R-mutant Ile106) using Lipofectamine 2000 (Life Technologies) according to the manufacturer's protocol. Transfected cells were harvested after 48 h and membranes prepared for receptor binding assays, as described (Abood et al., 1997).

Molecular Pharmacology Fast Forward. Published on May 26, 2015 as DOI: 10.1124/mol.115.098541
This article has not been copyedited and formatted. The final version may differ from this version.

Upper GI Motility Assay. Animal protocols were approved by the Institutional Animal Care and Use Committee of the NIAAA, NIH. Drugs (CB_1R antagonists, arachidonoyl-2'-chloroethylamine, and their combination) or vehicle were administered orally by gavage to male, 8-10 week-old C57Bl6/J mice 1 h prior to oral administration of the marker (10% charcoal suspension in 5% gum arabic). Thirty min later, mice were killed and the distance travelled by the head of the marker between the pylorus and the caecum was measured and expressed as percent of total length of the small intestine.

Hyperambulatory Activity. Locomotor activity of drug-naïve mice treated with an oral bolus dose of a CB_1R antagonist or vehicle was quantified by the number of disruptions of infrared beams in two dimensions in an activity chamber.

Molecular Pharmacology Fast Forward. Published on May 26, 2015 as DOI: 10.1124/mol.115.098541
This article has not been copyedited and formatted. The final version may differ from this version.

Results and Discussion

We synthesized compounds **14g** and **14h** (Fig. 1A) as described (Röver et al., 2013). The CB_1R binding affinity of the compounds was then analyzed in CHO cells transfected with the human CB_1R. The low nanomolar affinity of both compounds was similar to published values (Röver et al., 2013) and was also similar to that of the binding affinity of the reference compound rimonabant (Fig. 1B). In the same cells, **14g** and **14h** also displayed high potency as competitive inhibitors of CB_1R agonist-stimulated GTPγS activity, as derived from Schild-plots (Supplemental Figure 2). Because we wanted to test the compounds in a mouse model of DIO, we also tested their binding to mouse brain CB_1R. Surprisingly, the binding affinities of both **14g** and **14h** were 20- to 30-fold lower for mouse CB_1R compared to human CB_1R, whereas the affinity of rimonabant was comparable for mouse and human CB_1R (Fig. 1B). As this finding represents the first known example of a substantial species-specific difference in the affinity of a CB_1R antagonist, we also tested all three compounds for binding to the rat brain CB_1R, which differs in only one amino acid from the mouse CB_1R. In contrast, the human CB_1R, is one amino acid shorter and differs in an additional 13 amino acid residues from the mouse CB_1R. As seen in Fig. 1B, binding to the rat CB_1R revealed the same pattern as seen with the mouse CB_1R, i.e. rimonabant retained its high affinity, whereas **14g** and **14h** both had two orders of magnitude lower binding affinities and similar low potencies in a functional assay as inhibitors of agonist-stimulated GTPγS binding (Fig 1C).

Peak plasma concentrations of **14g** and **14h** in rats following an oral dose of 8-9 mg/kg were reported in the range of 1-3 μM with 96-98% of the ligands being plasma protein bound (Table 5 in (Röver et al., 2013)). Thus, the concentration of unbound ligand (20-60 nM) was well below the K_i for the rat or mouse CB_1R for both ligands, making it very unlikely that functional CB_1R blockade was achieved even at the somewhat higher dose of 30 mg/kg used in the earlier metabolic studies (Röver et al., 2013). To test this hypothesis, we treated normal control mice with a single oral dose of 10 or 30 mg/kg **14g** or **14h** or 10 mg/kg rimonabant and examined their effects in the upper GI motility assay (Izzo et al., 2001),

Molecular Pharmacology Fast Forward. Published on May 26, 2015 as DOI: 10.1124/mol.115.098541
This article has not been copyedited and formatted. The final version may differ from this version.

the industry standard for quantifying peripheral CB_1R blockade. As shown in Fig. 2A, upper GI motility as quantified by the distance traveled in 30 min by an oral charcoal bolus along the small intestine was profoundly inhibited by pretreatment with 10 mg/kg of the CB_1R agonist arachidonyl-2'-chloroethylamide, and the inhibition was completely prevented by rimonabant but remained unaffected by 10 or 30 mg/kg of either **14g** or **14h** (Fig. 2A). Similarly, rimonabant, but not **14g** or **14h**, caused hyperambulatory activity in drug-naïve wild-type but not $CB_1R^{-/-}$ mice (Fig. 2B). The hyperambulatory activity was associated with stereotypic behavior, such as scratching and grooming (not shown), and it is a recognized indicator of blockade of central CB_1R (Kunz et al., 2008; Tam et al., 2012; Tam et al., 2010). Thus, the reported inhibition of the modest diet-induced weight gain in rats by chronic treatment with the brain penetrant **14g** compound (Röver et al., 2013) may not be attributed to CB_1R blockade but rather to an off-target effect. Similarly, the lack of an inhibitory effect of **14h** is not relevant to the question of whether or not peripheral CB_1R contribute to the metabolic benefit of CB_1R blockade, as proposed (Röver et al., 2013).

However, the unique pharmacological property of compounds **14g** and **14h** to discriminate between human and rodent CB_1R could be exploited to gain new insight into the structure of the presumed binding pocket. We did molecular modeling of the CB_1R to explore the possible role of non-homologous amino acid residues of human versus rodent CB_1R that might account for the differential affinities of these ligands. As illustrated in Fig. 3A, compound **14g** can exist in solution in two conformations (**A** and **B**), due to a small energy difference, as indicated by quantum chemical calculations at the density functional level of B3LYP/6-31G*. Note that **14g** was constructed based on the X-ray structure of compound **14h** (Supplemental Figure 1). Of the two, conformer **B** rather than **A** is likely recognized by the human, rat or mouse CB_1R. This hypothesis is based on the comparison of the pharmacological properties of the core variants of the pyridine ring of **14g**, as indicated in Table 4 in (Röver et al., 2013). For example, conformer **A** of the compound **32a** is calculated to be 9.4 kcal/mol

Molecular Pharmacology Fast Forward. Published on May 26, 2015 as DOI: 10.1124/mol.115.098541
This article has not been copyedited and formatted. The final version may differ from this version.

more stable than conformer **B** of the same compound, as illustrated in Fig. 3B. This energy difference virtually assures that only **A** of **32a** exists in solution, and thus the reported significant decrease in K_i of **32a** (> 7000 nM for human CB_1R)(Röver et al., 2013) likely stems from the unfavorable orientation of the chlorophenyl and/or cyclo-propyl moiety of **A** in the binding pocket of CB_1R. A similar trend was observed for compounds **37a** and **51** (Röver et al., 2013). This in turn suggests that the conformer **B** of **14h** is also preferentially recognized by the CB_1R, as illustrated in Fig. 3C. It is noted that **14h** is crystallized as conformer **B**. In order to rationalize the differential affinity of **14g** and **14h** versus rimonabant towards the human, rat and mouse CB_1R, a model of human CB_1R was built based on the X-ray structure of a lipid GPCR (Hanson et al., 2012). Earlier models have been proposed based on the structures of bovine rhodopsin (Hurst et al., 2002; McAllister et al., 2003; Salo et al., 2004; Shim et al., 2003; Silvestri et al., 2008) or the β2-adrenergic receptor (Shim et al., 2012). The more recent structure used here as template affords a sequence alignment that is almost devoid of insertions and deletions. Thus, extracellular structure can be modeled readily for CB_1R, under the assumption that it is similar to that in the lipid GPCR (Data Supplement 1).

The mouse CB_1R is one amino acid longer than the human CB_1R, and the two differ in 13 additional amino acids, most of which are located at the N-terminal tail or in extracellular loops (Supplemental Figure 4). Our attention turned quickly to Ile105, because the side chain of this isoleucine points directly into the pocket of the modeled CB_1R (Fig. 4A). The three compounds of interest were manually docked into the human CB_1R model, taking into account the binding affinity data of rimonabant and other inverse agonists on CB_1R mutants, such as W279A (Sitkoff et al., 2011) and S383A (Kapur et al., 2007; Lin et al., 2008). Figure 4 depicts the putative binding modes of rimonabant and **14h**, and suggests that Ser383 can H-bond to the nitrogen of the pyridine ring of **14h**. Moreover, Ile105 in the human CB_1R is positioned to provide van der Waals interaction with the cyclohexanol of **14h**. The mouse and rat CB_1R have an equivalent methionine at position 106 (see Supplemental Figure 4), which likely

Molecular Pharmacology Fast Forward. Published on May 26, 2015 as DOI: 10.1124/mol.115.098541
This article has not been copyedited and formatted. The final version may differ from this version.

alters the protein-ligand interactions (Fig. 4B), and thus may explain the 20-fold lower K_i of **14h** for the rat compared to human CB_1R. Note that the 20-fold difference in K_i corresponds to 1.8 kcal/mol, which could result from the different interactions with Ile and Met at position 105/106 and/or the altered packing of adjacent residues.

To test the validity of this model, we mutated Ile105 in the human CB_1R to methionine, and Met106 in the mouse CB_1R to isoleucine, and transiently expressed the 2 native receptors and their mutants in HEK cells. Fig. 5 illustrates the results of radioligand displacement assays using membrane preparations from the 4 cell lines and rimonabant or compound **14h** as the unlabeled ligand. Whereas rimonabant had similar high affinity for the 2 native receptors and their mutants (Fig. 5A,B), the Ile105Met mutation of the human CB_1R resulted in a >100-fold decrease in the K_i of **14h** (Fig. 5C) and, conversely, the low affinity of **14h** to the native mouse CB_1R increased by two orders of magnitude in the Met106Ile mutants Fig. 5D). These findings clearly confirm the critical role of Ile105Met in the differential affinity of **14h** for the human versus mouse CB_1R, as postulated in our model. Since the structures of **14g** and **14h** are essentially identical except at 6-alkoxy **(**Supplemental Figure 3**)**, **14g** is expected to display similar differential affinity to the wild type and the mutant CB_1Rs.

The putative binding mode of rimonabant is depicted in Fig. 4A. This mode is compatible with the non-discriminatory binding affinity of rimonabant towards all three CB_1R orthologs. As compared to **14g** and **14h**, the aromatic portion of rimonabant was docked to be closer to the hydrophobic pocket formed by F268, W279 and W356, resulting in a sizable separation between Ile105 and the piperidine ring of rimonabant. As a consequence, neither Ile105 nor Met105 influences the binding affinity of rimonabant. Fig. 4B shows the positions of both the cyclohexanol of **14h** and the piperidine of rimonabant in the binding pocket of the human CB_1R.

Molecular Pharmacology Fast Forward. Published on May 26, 2015 as DOI: 10.1124/mol.115.098541
This article has not been copyedited and formatted. The final version may differ from this version.

In summary, an unprecedented, species-dependent difference in the binding affinity of a novel class of CB_1R antagonist to human versus rodent CB_1R was uncovered and its structural basis analyzed by molecular modeling based on the structure of a related lipid GPCR. The structural analysis suggested that the mutation of Ile to Met at position 105 most likely accounts for the lower affinity of 6-alkoxy-5-aryl-3-pyridincarboxamide CB_1R antagonists for rodent than for human CB_1R, and this hypothesis was then strongly supported by binding assays performed on site-directed mutants altered at this position. CB_1R antagonists have therapeutic potential in obesity/metabolic syndrome, and peripherally restricted analogs have been reported to retain metabolic efficacy with much reduced neuropsychiatric liability. The present findings highlight the importance of analyzing the interaction of CB_1R antagonists not only with the therapeutic target human CB_1R but also with the CB_1R of rodents used to generate preclinical proof of principle, in order to reach valid conclusions about mechanism of action.

Molecular Pharmacology Fast Forward. Published on May 26, 2015 as DOI: 10.1124/mol.115.098541
This article has not been copyedited and formatted. The final version may differ from this version.

Acknowledgements

The authors thank Dr. Mary E. Abood for providing the mouse *Cnr1* expression vector.

Author Contributions

Participated in research design: Kunos, Steinbach, Lee, Iyer, Cinar, Ikeda.

Conducted experiments: Cinar, Steinbach, Lee, Iyer, Puhl, Deschamps, Liu, Szanda, Godlewski.

Performed data analysis: Steinbach, Lee, Cinar, Iyer.

Wrote or contributed to the writing of the manuscript: Kunos, Steinbach, Lee, Iyer, Cinar.

References

Abood ME, Ditto KE, Noel MA, Showalter VM and Tao Q (1997) Isolation and expression of a mouse CB1 cannabinoid receptor gene. Comparison of binding properties with those of native CB1 receptors in mouse brain and N18TG2 neuroblastoma cells. *Biochem Pharmacol* **53**(2): 207-214.

Bluher M, Engeli S, Kloting N, Berndt J, Fasshauer M, Batkai S, Pacher P, Schon MR, Jordan J and Stumvoll M (2006) Dysregulation of the peripheral and adipose tissue endocannabinoid system in human abdominal obesity. *Diabetes* **55**(11): 3053-3060.

Collins S, Martin TL, Surwit RS and Robidoux J (2004) Genetic vulnerability to diet-induced obesity in the C57BL/6J mouse: physiological and molecular characteristics. *Physiol Behav* **81**(2): 243-248.

Compton DR, Rice KC, De Costa BR, Razdan RK, Melvin LS, Johnson MR, Martin BR. (1993) Cannabinoid structure-activity relationships: correlation of receptor binding and in vivo activities. *J Pharmacol Exp Ther* **265**(1):218-226.

Cota D, Marsicano G, Tschop M, Grubler Y, Flachskamm C, Schubert M, Auer D, Yassouridis A, Thone-Reineke C, Ortmann S, Tomassoni F, Cervino C, Nisoli E, Linthorst AC, Pasquali R, Lutz B, Stalla GK and Pagotto U (2003) The endogenous cannabinoid system affects energy balance via central orexigenic drive and peripheral lipogenesis. *J Clin Invest* **112**(3): 423-431.

Despres JP, Golay A and Sjostrom L (2005) Effects of rimonabant on metabolic risk factors in overweight patients with dyslipidemia. *N Engl J Med* **353**(20): 2121-2134.

Flamment M, Gueguen N, Wetterwald C, Simard G, Malthiery Y and Ducluzeau PH (2009) Effects of the cannabinoid CB1 antagonist rimonabant on hepatic mitochondrial function in rats fed a high-fat diet. *Am J Physiol Endocrinol Metab* **297**(5): E1162-1170.

Griffin G, Atkinson PJ, Showalter VM, Martin BR and Abood ME (1998) Evaluation of cannabinoid receptor agonists and antagonists using the guanosine-5'-O-(3-[35S]thio)-triphosphate binding assay in rat cerebellar membranes. *J Pharmacol Exp Ther.* **285**(2):553-560.

Govaerts SJ, Hermans E and Lambert DM (2004) Comparison of cannabinoid ligands affinities and efficacies in murine tissues and in transfected cells expressing human recombinant cannabinoid receptors. *Eur J Pharm Sci* **23**(3): 233-243.

Hanson MA, Roth CB, Jo E, Griffith MT, Scott FL, Reinhart G, Desale H, Clemons B, Cahalan SM, Schuerer SC, Sanna MG, Han GW, Kuhn P, Rosen H and Stevens RC (2012) Crystal structure of a lipid G protein-coupled receptor. *Science* **335**(6070): 851-855.

Hurst DP, Lynch DL, Barnett-Norris J, Hyatt SM, Seltzman HH, Zhong M, Song ZH, Nie J, Lewis D and Reggio PH (2002) N-(piperidin-1-yl)-5-(4-chlorophenyl)-1-(2,4-dichlorophenyl)-4-methyl-1H-

pyrazole -3-carboxamide (SR141716A) interaction with LYS 3.28(192) is crucial for its inverse agonism at the cannabinoid CB1 receptor. *Mol Pharmacol* **62**(6): 1274-1287.

Izzo AA, Fezza F, Capasso R, Bisogno T, Pinto L, Iuvone T, Esposito G, Mascolo N, Di Marzo V and Capasso F (2001) Cannabinoid CB1-receptor mediated regulation of gastrointestinal motility in mice in a model of intestinal inflammation. *Br J Pharmacol* **134**(3): 563-570.

Jourdan T, Godlewski G, Cinar R, Bertola A, Szanda G, Liu J, Tam J, Han T, Mukhopadhyay B, Skarulis MC, Ju C, Aouadi M, Czech MP and Kunos G (2013) Activation of the Nlrp3 inflammasome in infiltrating macrophages by endocannabinoids mediates beta cell loss in type 2 diabetes. *Nat Med* **19**(9): 1132-1140.

Kapur A, Hurst DP, Fleischer D, Whitnell R, Thakur GA, Makriyannis A, Reggio PH and Abood ME (2007) Mutation studies of Ser7.39 and Ser2.60 in the human CB1 cannabinoid receptor: evidence for a serine-induced bend in CB1 transmembrane helix 7. *Mol Pharmacol* **71**(6): 1512-1524.

Kim W, Doyle ME, Liu Z, Lao Q, Shin YK, Carlson OD, Kim HS, Thomas S, Napora JK, Lee EK, Moaddel R, Wang Y, Maudsley S, Martin B, Kulkarni RN and Egan JM (2011) Cannabinoids inhibit insulin receptor signaling in pancreatic beta-cells. *Diabetes* **60**(4): 1198-1209.

Kraulis PJ (1991) MOLSCRIPT: a program to produce both detailed and schematic plots of protein structures. *J Appl Crystallogr* **24**:946-950.

Kunz I, Meier MK, Bourson A, Fisseha M and Schilling W (2008) Effects of rimonabant, a cannabinoid CB1 receptor ligand, on energy expenditure in lean rats. *Int J Obes (Lond)* **32**(5): 863-870.

Le Foll B, Gorelick DA and Goldberg SR (2009) The future of endocannabinoid-oriented clinical research after CB1 antagonists. *Psychopharmacology (Berl)* **205**(1): 171-174.

Lin LS, Ha S, Ball RG, Tsou NN, Castonguay LA, Doss GA, Fong TM, Shen CP, Xiao JC, Goulet MT and Hagmann WK (2008) Conformational analysis and receptor docking of N-[(1S,2S)-3-(4-chlorophenyl)-2-(3-cyanophenyl)-1-methylpropyl]-2-methyl-2-{[5-(t rifluoromethyl)pyridin-2-yl]oxy}propanamide (taranabant, MK-0364), a novel, acyclic cannabinoid-1 receptor inverse agonist. *J Med Chem* **51**(7): 2108-2114.

Liu YL, Connoley IP, Wilson CA and Stock MJ (2005) Effects of the cannabinoid CB1 receptor antagonist SR141716 on oxygen consumption and soleus muscle glucose uptake in Lep(ob)/Lep(ob) mice. *Int J Obes (Lond)* **29**(2): 183-187.

McAllister SD, Rizvi G, Anavi-Goffer S, Hurst DP, Barnett-Norris J, Lynch DL, Reggio PH and Abood ME (2003) An aromatic microdomain at the cannabinoid CB(1) receptor constitutes an agonist/inverse agonist binding region. *J Med Chem* **46**(24): 5139-5152.

Merritt EA and Bacon DJ (1997) Raster3D: photorealistic molecular graphics. *Method Enzymol* **277**:505-524.

Osei-Hyiaman D, DePetrillo M, Pacher P, Liu J, Radaeva S, Batkai S, Harvey-White J, Mackie K, Offertaler L, Wang L and Kunos G (2005) Endocannabinoid activation at hepatic CB1 receptors stimulates fatty acid synthesis and contributes to diet-induced obesity. *J Clin Invest* **115**(5): 1298-1305.

Pacher P, Batkai S and Kunos G (2006) The endocannabinoid system as an emerging target of pharmacotherapy. *Pharmacol Rev* **58**(3): 389-462.

Perrin MA, Bauer M, Barrio M, Tamarit JL, Ceolin R and Rietveld IB (2013) Rimonabant dimorphism and its pressure-temperature phase diagram: a delicate case of overall monotropic behavior. *Journal of pharmaceutical sciences* **102**(7): 2311-2321.

Pi-Sunyer FX, Aronne LJ, Heshmati HM, Devin J and Rosenstock J (2006) Effect of rimonabant, a cannabinoid-1 receptor blocker, on weight and cardiometabolic risk factors in overweight or obese patients: RIO-North America: a randomized controlled trial. *Jama* **295**(7): 761-775.

Röver S, Andjelkovic M, Benardeau A, Chaput E, Guba W, Hebeisen P, Mohr S, Nettekoven M, Obst U, Richter WF, Ullmer C, Waldmeier P and Wright MB (2013) 6-Alkoxy-5-aryl-3-pyridinecarboxamides, a new series of bioavailable cannabinoid receptor type 1 (CB1) antagonists including peripherally selective compounds. *J Med Chem* **56**(24): 9874-9896.

Salo OM, Lahtela-Kakkonen M, Gynther J, Jarvinen T and Poso A (2004) Development of a 3D model for the human cannabinoid CB1 receptor. *J Med Chem* **47**(12): 3048-3057.

Shim JY, Bertalovitz AC and Kendall DA (2012) Probing the interaction of SR141716A with the CB1 receptor. *J Biol Chem* **287**(46): 38741-38754.

Shim JY, Welsh WJ and Howlett AC (2003) Homology model of the CB1 cannabinoid receptor: sites critical for nonclassical cannabinoid agonist interaction. *Biopolymers* **71**(2): 169-189.

Silvestri R, Cascio MG, La Regina G, Piscitelli F, Lavecchia A, Brizzi A, Pasquini S, Botta M, Novellino E, Di Marzo V and Corelli F (2008) Synthesis, cannabinoid receptor affinity, and molecular modeling studies of substituted 1-aryl-5-(1H-pyrrol-1-yl)-1H-pyrazole-3-carboxamides. *J Med Chem* **51**(6): 1560-1576.

Sim-Selley LJ, Brunk LK and Selley DE (2001) Inhibitory effects of SR141716A on G-protein activation in rat brain. *Eur J Pharmacol* **414**(2-3): 135-143.

Sitkoff DF, Lee N, Ellsworth BA, Huang Q, Kang L, Baska R, Huang Y, Sun C, Pendri A, Malley MF, Scaringe RP, Gougoutas JZ, Reggio PH, Ewing WR, Pelleymounter MA and Carlson KE (2011) Cannabinoid CB(1) receptor ligand binding and function examined through mutagenesis studies of F200 and S383. *Eur J Pharmacol* **651**(1-3): 9-17.

Tam J, Cinar R, Liu J, Godlewski G, Wesley D, Jourdan T, Szanda G, Mukhopadhyay B, Chedester L, Liow JS, Innis RB, Cheng K, Rice KC, Deschamps JR, Chorvat RJ, McElroy JF and Kunos G (2012) Peripheral cannabinoid-1 receptor inverse agonism reduces obesity by reversing leptin resistance. *Cell Metab* **16**(2): 167-179.

Tam J, Vemuri VK, Liu J, Batkai S, Mukhopadhyay B, Godlewski G, Osei-Hyiaman D, Ohnuma S, Ambudkar SV, Pickel J, Makriyannis A and Kunos G (2010) Peripheral CB1 cannabinoid receptor blockade improves cardiometabolic risk in mouse models of obesity. *J Clin Invest* **120**(8): 2953-2966.

Thomas BF, Francisco ME, Seltzman HH, Thomas JB, Fix SE, Schulz AK, Gilliam AF, Pertwee RG and Stevenson LA (2005) Synthesis of long-chain amide analogs of the cannabinoid CB1 receptor antagonist N-(piperidinyl)-5-(4-chlorophenyl)-1-(2,4-dichlorophenyl)-4-methyl-1H-pyrazole-3-carboxamide (SR141716) with unique binding selectivities and pharmacological activities. *Bioorg Med Chem* **13**(18): 5463-5474.

Molecular Pharmacology Fast Forward. Published on May 26, 2015 as DOI: 10.1124/mol.115.098541
This article has not been copyedited and formatted. The final version may differ from this version.

Footnotes.

M.R.I. and R.C. are co-first authors of this paper

This study was supported by the Intramural Research Programs of the National Institute of Alcohol Abuse and Alcoholism and of the Center for Molecular Modeling, Division of Computational Bioscience, National Institutes of Health. The X-ray crystallographic work was supported by the National Institute on Drug Abuse through Interagency Agreement [Y1-DA1101] with the Naval Research Laboratory.

Molecular Pharmacology Fast Forward. Published on May 26, 2015 as DOI: 10.1124/mol.115.098541
This article has not been copyedited and formatted. The final version may differ from this version.

Figure Legends

Fig. 1. Chemical structure (A), binding affinity (B) and inhibitory potency (C) of rimonabant and compounds **14g** and **14h** to human, rat and mouse CB_1 receptors. K_i values for binding and functional antagonism were determined as described in Methods. Points and vertical bars represent means ± SE from 4-6 independent assays. Hill slopes were not significantly different from 1.0. For panel B, specific binding (fmol/mg protein) in the absence of competitor was 2236 ± 30 (hCB_1CHO), 225 ± 6 (rat brain), or 222 ± 14 (mouse brain), and was defined as 100%. For panel C, basal GTPγS specific binding was 187 ± 5 fmol/mg protein.

Fig. 2. In vivo assays to assess peripheral and central CB_1R blockade. A: the upper GI motility assay was conducted as described in Methods. Note that rimonabant, but not compound **14g** or **14h**, block the CB_1R agonist (Farghali, #2150)-induced inhibition of upper GI motility. Columns and vertical bars represent means ± SE from 4 separate experiments. *, #: Significant difference ($P<0.01$) from values in vehicle + vehicle-treated or vehicle + ACEA-treated mice, respectively. B,C: ambulatory activity in drug-naïve mice was quantified as described in Methods. Note that rimonabant, but not **14g** or **14h**, causes long lasting hyperambulatory activity in wild-type mice (B) but not in $CB_1R^{-/-}$ mice (C).

Fig. 3. Geometry optimized A and B conformers of **14g** (A), **32a** (B), and **14h** (C), at the level of B3LYP/6-31G* in the gaseous phase. Values in parentheses represent the Gibbs free energy in kcal/mol relative to that of A at 298.15 K. The conversion of B to A was done by varying the dihedral angle φ centered on the C-C bond as indicated by the arrow. Atom coloring: white, hydrogen; green, carbon; dark green, chlorine; blue, nitrogen; red, oxygen.

Fig. 4. Model of rimonabant and **14h** binding to human CB_1R. A) The homology model of human CB_1R is depicted with the protein backbone colored by sequence identity to the template X-ray structure (gold where identical, light blue where different). The side chains of Ile105, Phe268, Trp279, and Trp356 are shown as space-filling, and those of Glu94, Val110, Ile175, Arg186, Glu258, and His270 (where human CB_1R differs from rat and/or mouse CB_1R) are shown as ball-and-stick. Rimonabant and **14h** are shown manually docked in the pocket of the receptor as ball-and-stick with carbon atoms colored green and gray, respectively. B) Close-up, rotated view of the docked ligands in the receptor pocket, colored as in (A). This figure was created using the programs MolScript (Kraulis, 1991) and Raster3D (Merritt and Bacon, 1997).

Fig. 5. Binding of rimonabant (A, B) and compound **14h** (C, D) to wild-type and mutated human and mouse CB_1R. Radioligand binding displacement by compound **14h** was tested using plasma membrane

Molecular Pharmacology Fast Forward. Published on May 26, 2015 as DOI: 10.1124/mol.115.098541
This article has not been copyedited and formatted. The final version may differ from this version.

preparations from CHO cells transfected with cDNA for the wild-type human or mouse CB_1R, with an Ile105Met mutant of human CB_1R, or a Met106Ile mutant of mouse CB_1R. [^{3}H]CP55940 (2 nM) was used as the labeled ligand. Points and vertical bars are means ± SE from 4 independent assays.

Figure 1

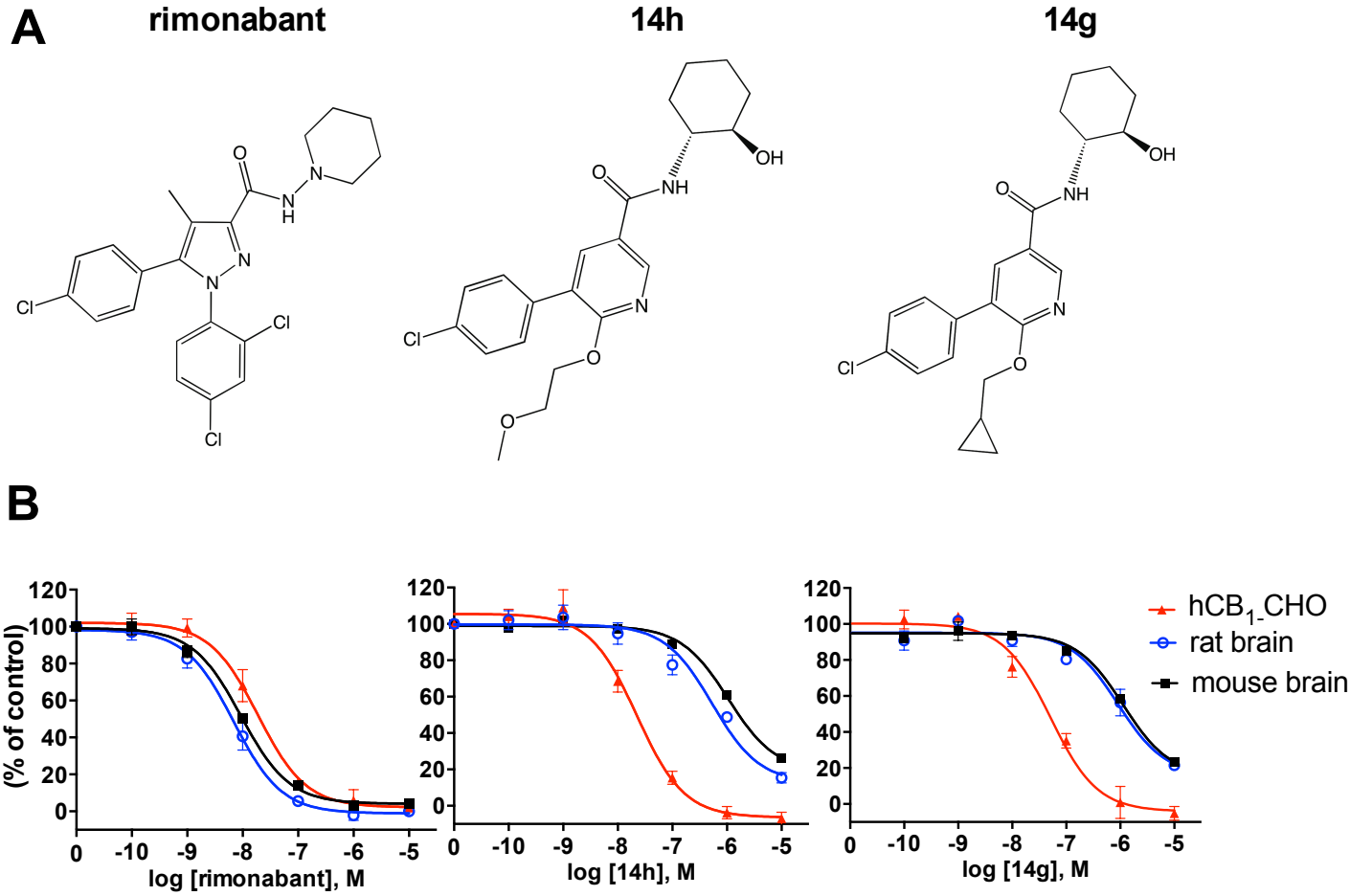

	rat brain K_i [nM]	mouse brain K_i [nM]	hCB$_1$-CHO K_i [nM]
Rimonabant	3 ± 1	4 ± 0.5	9 ± 2
14h	244 ± 7	469 ± 9	10 ± 2
14g	392 ± 2	485 ± 1.3	21 ± 1.4

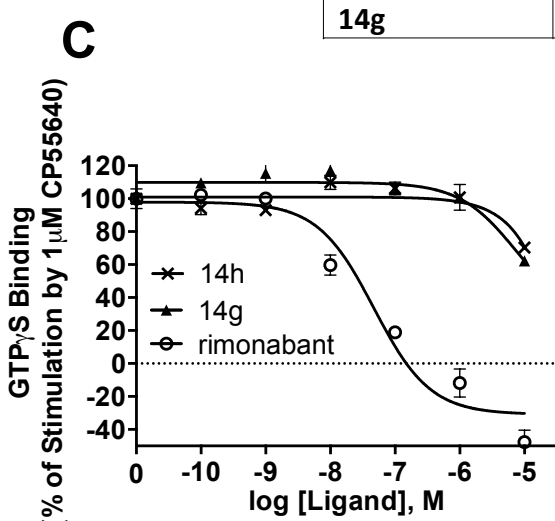

Figure 2

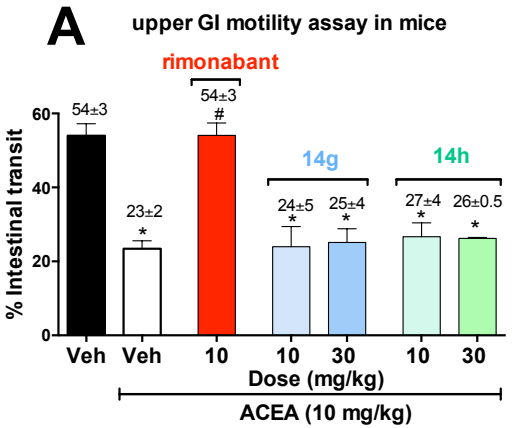
A
upper GI motility assay in mice
rimonabant
14g
14h
% Intestinal transit
54±3
23±2
54±3
#
24±5
25±4
27±4
26±0.5
Veh
Veh
10
10
30
10
30
Dose (mg/kg)
ACEA (10 mg/kg)

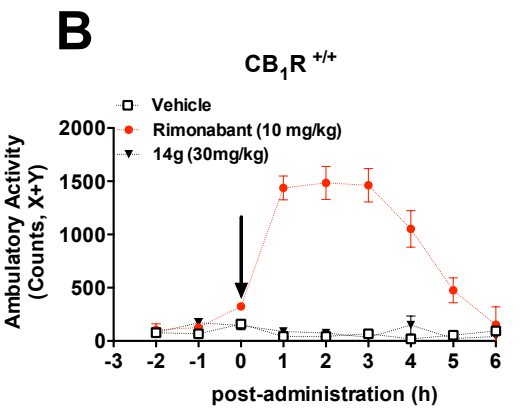
B
CB1R +/+
Vehicle
Rimonabant (10 mg/kg)
14g (30mg/kg)
Ambulatory Activity (Counts, X+Y)
post-administration (h)

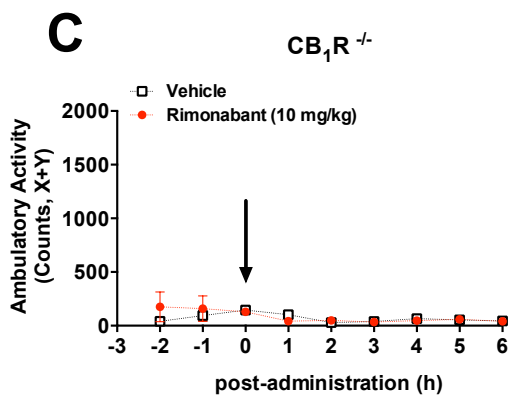
C
CB1R -/-
Vehicle
Rimonabant (10 mg/kg)
Ambulatory Activity (Counts, X+Y)
post-administration (h)

Figure 3

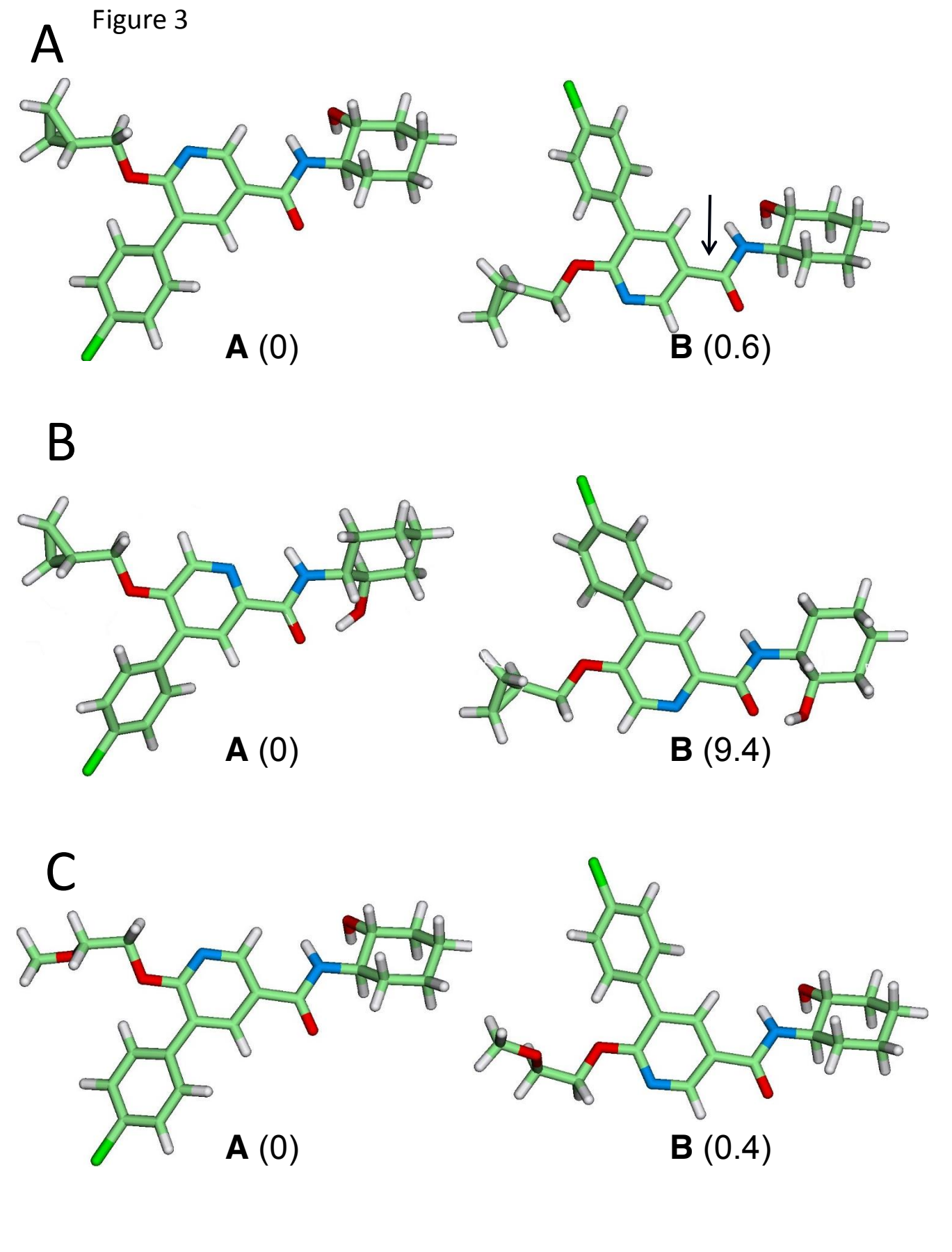

Molecular Pharmacology Fast Forward. Published on May 26, 2015 as DOI: 10.1124/mol.115.098541
This article has not been copyedited and formatted. The final version may differ from this version.

Figure 4

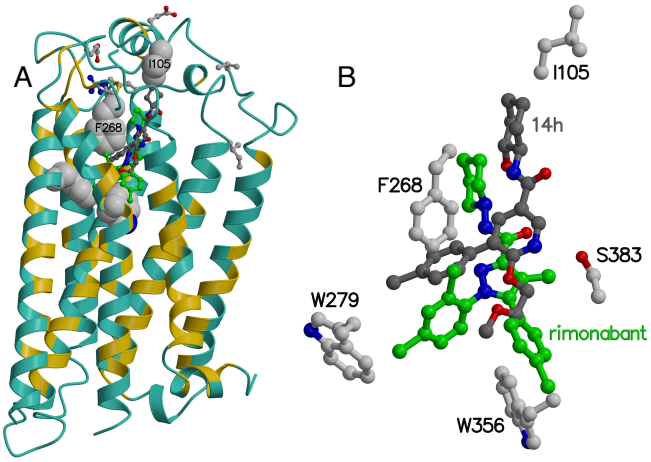

Figure 5

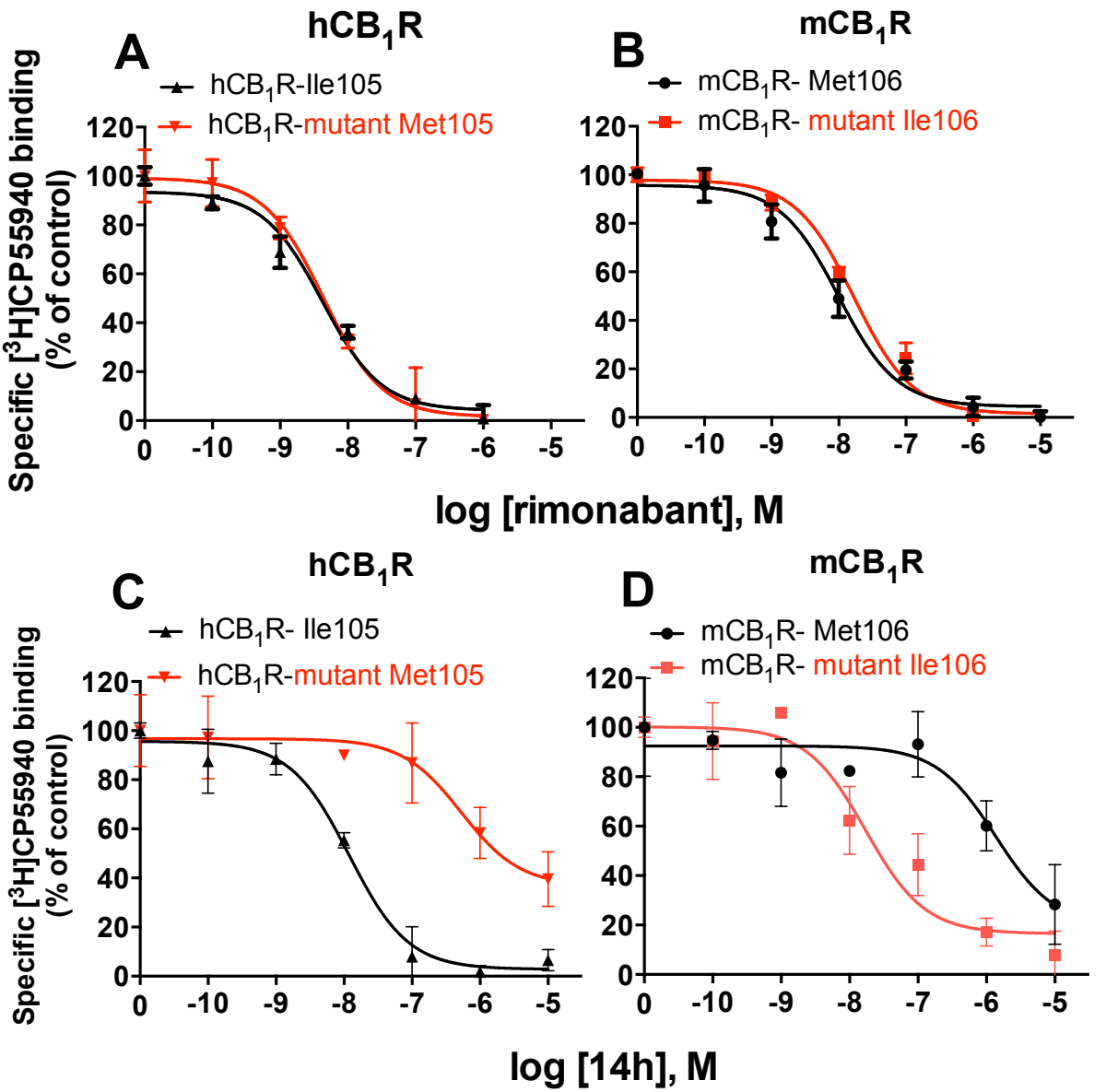

	hCB$_1$R I105	hCB$_1$R mutant M105	mCB$_1$R M106	mCB$_1$R mutant I106
Compound 14h Ki [nM]	5 ± 1	771 ± 27	614 ± 22	8 ± 4
Rimonabant Ki [nM]	1.8 ± 0.5	1.9 ± 0.6	3.4 ± 0.3	3.4 ± 0.2